Solvent-free electrospinning of liquid polybutadienes and their in-situ photocuring

Solvent-free electrospinning of liquid polybutadienes and their *in-situ* photocuring

P. Kianfar[1,*], H. Q. Nguyen Trieu[1,#], S. Dalle Vacche[1], L. Tsantilis[3], R. Bongiovanni[1,2], A. Vitale[1,2,*]

[1] Department of Applied Science and Technology, Politecnico di Torino, 10129 Torino, Italy
[2] INSTM – Politecnico di Torino Research Unit, 50121 Firenze, Italy
[3] Department of Environment, Land and Infrastructure Engineering, Politecnico di Torino, 10129 Torino, Italy
[#] Present address: Samyang Engineering Plastics Vietnam LLC, Nhon Trach District, Dong Nai Province, Vietnam

*Correspondence to: parnian.kianfar@polito.it; alessandra.vitale@polito.it

A single-step approach to rapidly convert low molecular weight polybutadienes into fine rubber crosslinked fibers and nonwoven mats without using any heat or solvent was described. This environmentally friendly method consisted in the electrospinning at room temperature of liquid polybutadiene and polybutadiene-*graft*-maleic anhydride polymers without any solvent; the flying jet was irradiated to trigger the *in-situ* curing of the forming fibers at ambient conditions, obtaining a good control over the fibrous morphology and enhancing the performance of the membranes. The kinetics of the photo-crosslinking reaction was studied through FT-IR spectroscopy. Liquid polybutadiene-*graft*-maleic anhydride polymers demonstrated a faster rate of photocuring, compared to neat polybutadienes. In order to further speed up the reaction, a thiol-based crosslinker and a photoinitiator were introduced into the formulations. The photo-induced crosslinking was more efficient as different reactions concomitantly took place: besides the thiol-ene crosslinking involving the multifunctional thiol crosslinker, the oxidation of the polybutadiene chains and the esterification of the maleic anhydride moieties occurred. Moreover, a polar additive was used to control the electrospinning process by lowering the viscosity and increasing the electrical conductivity. The structural, thermal and surface properties of the fabricated polybutadiene-based electrospun membranes were assessed. The membranes exhibited an excellent morphology stability, high insolubility, good thermal properties and a pronounced hydrophobic character.

Keywords: Liquid polybutadienes; Electrospinning; Photocuring; Photo-crosslinking; Rubber fibers

Introduction

Electrospinning is a fascinating technique for the fabrication of fine fibers ranging from several tens of nanometers to many micrometers with relatively straightforward tunability [1–4]. In the last decades, it has thus gained much attention in a wide range of applications, from filtration to environmental and energy fields [5], catalysis [6], sensing [7], textile, biomedical devices [8] and many more [9–12]. Electrospinning requires the application of a high electrical field (10–30 kV) to a polymeric solvent solution to form a jet; a rapid evaporation of the solvent allows the formation of solid polymer fibers on the collector [13]. As this technology usually employs large quantities of volatile solvents (i.e., 80–95 wt.%), drawbacks can be the difficulty in solvent recycling/recovery, the toxicity of the employed solvents, and a low mass throughput due to solvent evaporation. Alternatively, melt electrospinning has been developed [14–16], guaranteeing a higher productivity compared to solvent electrospinning. However, as polymer melts are employed, high operational temperatures must be adopted; moreover, the high viscosity and the low conductivity of polymer melts limit the control of the fiber size and larger diameters are generally obtained [14,17,18].

Another strategy is the electrospinning of reactive monomers/oligomers and their *in-situ* polymerization/crosslinking: it is an extremely interesting and sustainable way to form fine fibers without using solvents or heat [19]. In this case, a suitable chemistry assuring a fast reaction rate compatible with typical electrospinning fiber process speeds (>1 m/s) has to be identified. Photo-induced crosslinking may be appropriate, as it is characterized by very short conversion times [20]. Moreover, it has other advantages, namely the low-energy consumption, the ambient temperature operations, and the selective curing with a precise control both in time and space. Photo-crosslinking has been applied to preformed fibers obtained by solution electrospinning of various polymeric systems, such as polyethylene oxide, (meth)acrylated gelatin and unsaturated polyesters [21–28]. Correspondingly, greener approaches of *in-situ* photopolymerization/photocuring during electrospinning as well as other fiber spinning processes (i.e., melt blowing and centrifugal spinning) without using any solvent and thus raising less environmental and health concern have also been proposed in the literature. Such works are mainly based on the photopolymerization of thiol-ene and acrylic monomers [29–36], including both synthesized on purpose and commercial products. Herein, we prepared electrospun rubber fibers and fibrous membranes using low molecular weight polybutadienes and polybutadienes grafted with maleic anhydride that are commercially available and

currently employed as mold release additives and adhesion promoters. Being liquid, they can be electrospun without using any solvent; to obtain solid fibers and achieve thermo-mechanical performances comparable to those of high molecular weight polybutadiene polymers (processed by solution electrospinning) [28,37–42], the investigated systems were subjected to curing.

It is well known that liquid polybutadienes can be crosslinked by an oxidative process by heating at 160–200 °C, eventually adding metallic catalysts [43,44]; this reaction is widely employed to dry coatings. Moreover, when liquid polybutadienes are modified by maleic anhydride, the thermal curing reaction can take place using appropriate amine crosslinkers and reactive polyols [45,46]. However, being highly unsaturated (i.e., rich in C=C double bonds), both polybutadienes and maleinized polybutadienes are also potential candidates for photocuring processes, which are much faster. Photo-induced reactions can happen due to the abstraction of allylic hydrogen atoms in the α position of the double bonds when the material is subjected to UV radiation [47,48]: free radicals are generated and trigger propagation reactions. Moreover, a radical-type photoinitiator and a multifunctional thiol crosslinker may be used to further speed up the photo-induced crosslinking reaction. Photoinitiated thiol-ene polymerization, in fact, proceeds by a radical-mediated step-growth mechanism, which is propagated by a chain transfer reaction involving the thiyl radicals ($RS^{\bullet}$) [49–51], assuring high efficiency under ambient conditions (i.e., air and room temperature environment) [52].

In this work, first the photo-crosslinking reaction of liquid polybutadienes, with and without crosslinker and photoinitiator, and its efficiency were studied through Fourier Transform Infrared (FT-IR) spectroscopy and insoluble fraction measurements. The liquid polybutadiene-based formulation was optimized for electrospinning, especially in terms of reaction rate, viscosity and conductivity. Efficiently photo-crosslinked electrospun mats with an excellent morphology stability, high insolubility, good thermal properties and a pronounced hydrophobic character were obtained. Thus, we demonstrated that by combining electrospinning and *in-situ* photo-induced crosslinking liquid polybutadienes can be successfully converted into stable rubber crosslinked fibers and nonwoven mats without using any heat, solvent, or other volatile component. This is particularly interesting as the polybutadiene unsaturations are generally considered fairly unreactive under light irradiation. The chosen approach, besides being environmentally friendly, proved to be efficient, being a single-step process able to form at room temperature in few seconds solid rubber fine fibers with good performances.

Materials and methods

Materials

Liquid polybutadienes (Lithene ultra® N4-5000) and liquid polybutadienes grafted with maleic anhydride (Lithene ultra® N4-5000-10MA and N4-5000-15MA) were kindly provided by Synthomer. To simplify the names of the samples, the following abbreviations are used: PB, PB-10MA and PB-15MA for Lithene ultra® N4-5000, N4-5000-10MA and N4-5000-15MA, respectively. The representative chemical structure of PB and a polybutadiene grafted with maleic anhydride (maleinized PB) are reported in Figure 1. Table 1 summarizes the main properties of the liquid polybutadienes as provided by the supplier.

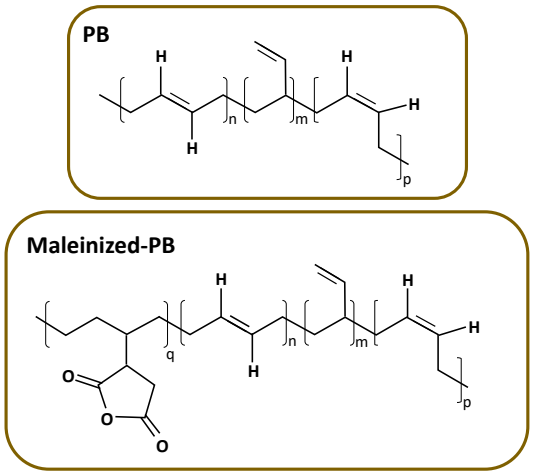

Figure 1. Chemical structure of polybutadiene (PB) and polybutadiene-*graft*-maleic anhydride (maleinized PB).

Table 1. Properties of the investigated polybutadienes.

Sample	M_n (g/mol)	Grafted maleic anhydride (wt.%)	Vinyl 1,2 content (%)	Viscosity @25°C (dPa s)	f' (functional groups/chain)	T_g by DSC (°C)
PB	5000	0	10-20	30-50	-	-92.5
PB-10MA	5500	10	10-20	250-600	5.1	-84.4
PB-15MA	5750	15	10-20	1200-2200	7.7	-79.1

Trimethylbenzoyl diphenylphosphine oxide (TPO), trimethylolpropane tris(3-mercaptopropionate) (≥95 %) (TRIS) and oleic acid (OA) from Sigma-Aldrich were used as photoinitiator, crosslinking agent and polar electrospinning additive, respectively.

All other chemicals were acquired from Sigma-Aldrich.

Photocured electrospun mats preparation

Electrospinning was performed by an E-fiber electrospinning system SKE apparatus in horizontal setup, equipped with a high voltage power supply, a programmable syringe pump and a grounded aluminum foil as collector. A syringe tip with diameter of 1 mm was employed during electrospinning. Electrospinning was conducted at environmental conditions by applying a voltage of 14–16 kV, a flow rate of 0.1–0.4 ml/h, and a tip-to-collector working distance of 6 cm. During electrospinning, the liquid polymer jet as well as the collector were irradiated (at room temperature) by means of a high-pressure mercury-xenon lamp equipped with an optical fiber (LIGHTNINGCURE^{TM} Spotlight source LC8, Hamamatsu), with an intensity of 280 mW/cm^2 on the collector. The UV light intensity was measured by a UV Power Puck® II from EIT® Instrument Markets. The electrospun mats were then characterized either keeping them on the collector or as free-standing membranes after detachment from the substrate.

Photocured film preparation

Plain films with a thickness of 12 μm were prepared by coating a glass substrate with the liquid polybutadiene, using a wire-wound applicator. The curing process was performed at room temperature by means of a high-pressure mercury-xenon lamp equipped with an optical fiber (LIGHTNINGCURE^{TM} Spotlight source LC8, Hamamatsu). The UV light intensity was measured by a UV Power Puck® II from EIT® Instrument Markets and was set to 280 mW/cm^2. The polymer films were irradiated for different exposure times until solidification.

Characterization

The tack-free time of 12 μm thick flat films coated on a glass slide and irradiated for different time lengths was assessed by pressing the thumb on the specimen surface and turning it through an angle of 90° in the plane of the film. The film was considered tack-free when there was no mark left on the specimen surface, no trace of sticky surface on the thumb, as well as no loosening, detachment, wrinkling, or other evidence of distortion of the film (i.e., dry-to-handle

time, as in ASTM D1640/D1640M) [53]. These experiments were conducted at room temperature (i.e., 23 °C), and the test was repeated on at least three samples. The error could be estimated to be <10 %.

In order to study the absorption of pure materials in UV-Vis range, UV–Vis spectroscopy was performed. Absorbance spectra were collected by means of a 6850 Jenway UV–Vis spectrophotometer in the range of 200-700 nm with a resolution of 0.2 nm. 12 µm thick flat films were coated on a quartz slide and subjected to the measurement while a clean quartz slide was used as the reference.

For assessing the chemical bonds and compositions of thin films before and after UV curing, FT-IR spectroscopy analyses were performed using a Thermo Fisher Scientific Nicolet™ iS50 spectrometer in transmission mode in the spectral range of 4000–400 cm^{-1}. 12 µm thick films on a silicon wafer as substrate were irradiated for different time lengths and analyzed by FT-IR spectroscopy. All spectra were taken by an accumulation of 32 scans with a resolution of 4 cm^{-1}. The conversion of the reactive groups was calculated based on Eq. 1:

$$Conversion\ \% = \left(1 - \frac{A_t}{A_0}\right) \times 100 \qquad \text{(Eq. 1)}$$

Where A_t is the area of the peak of reactive groups at time t of irradiation, and A_0 is the area of the same peak band at time 0 of irradiation. The double bond conversion was monitored through the C=C peak band at 1650 cm^{-1}, while the opening of the maleic anhydride ring was controlled by tracking the disappearance of the two peaks at 1780 cm^{-1} and 1864 cm^{-1}, assigned to the C=O groups attached to the ring.

The insoluble fraction of photocured samples after their complete solidification was measured by gel content experiments, evaluating the weight loss after 24 h extraction by toluene at room temperature.

Photo-rheology experiments were performed on liquid samples using a Modular Compact Rheometer MCR 302 (Anton Paar) equipped with a parallel-plate configuration with diameter of 25 mm and a quartz bottom glass. The gap between the two plates was set to 100 µm. A high-pressure mercury-xenon lamp equipped with an optical fiber (LIGHTNINGCURE™ Spotlight source LC8, Hamamatsu), placed below the quartz plate, was used to irradiate the samples from the bottom part with a UV intensity of 100 mW/cm^2 (measured by an EIT® Instrument Markets UV Power Puck® II radiometer). Initially, in order to determine the linear

viscoelastic regime, an amplitude sweep experiment with a strain (γ) ramp ranging from 0.01 % to 100 % at a constant frequency of 0.1 Hz was performed. Then, time sweep experiments were carried out in the linear viscoelastic region at a constant γ = 0.1% and a constant frequency of 0.1 Hz. The UV lamp was switched on after 60 s of data acquisition. The evolution of the elastic storage modulus G' and the loss modulus G" with time was monitored until the occurrence of the gel point. All experiments were performed at 25 °C.

The viscosity of the investigated liquid mixtures for electrospinning was measured using a Modular Compact Rheometer MCR 302 (Anton Paar) equipped with a parallel-plate configuration, with diameter of 25 mm. The shear viscosity was measured over a wide range of shear rate (0.01–100 s^{-1}) at 25 °C and setting 1 mm as the gap between the upper plate and the platform.

The electrospun fiber morphology was monitored by means of an Olympus BX53M optical microscope. Fiber size distributions were obtained by using ImageJ software; approximately 100 measurements/sample were performed. The thermal stability of the fiber morphology was evaluated by heating an electrospun photocured mat at 40 °C, 60 °C, 80 °C and 100 °C for 20 min for each temperature: samples were imaged and analyzed as previously described.

Thermal stability of the electrospun membranes was evaluated by thermogravimetric analysis (TGA), using a Mettler Toledo TGA/SDTA 851e apparatus. Scans were made from 25 °C to 800 °C with a heating rate of 10 °C/min, under a N_2 flux to prevent thermos-oxidative processes.

The viscoelastic behavior of the fibrous membranes was determined by using a dynamic mechanical thermal analysis (DMTA) instrument from Triton Technology. Measurements were conducted in dynamic tensile mode using a temperature sweep method, from -100 °C to 25 °C, at a fixed frequency of 1 Hz with heating rate of 3 °C/min. Samples of approximately 10 mm x 7 mm x 0.4 mm were cut from the collected membranes and placed directly into the grips. The glass transition temperature (T_g) was measured as the maximum of the tan δ curve.

The wettability of the fibrous membranes was investigated by performing static contact angle measurements by means of a FTA 1000C instrument equipped with a video camera and image analyzer, at room temperature with the sessile drop technique. Three to five measurements were performed on each fibrous sample placing the liquid drops in different parts of the sample

surface: the mean value and the error were determined. The probe liquids were water and hexadecane, whose surface tensions are 72.1 mN/m and 28.1 mN/m, respectively.

Results and discussion

With the aim of producing rubber fibrous membranes in a sustainable way, a low molecular weight polybutadiene polymer at the liquid state (PB) and its homologues grafted with maleic anhydride (i.e., maleinized polybutadiene PB-10MA and PB-15MA) were electrospun without the use of any solvent at room temperature. Electrospinning was combined with *in-situ* irradiation at ambient conditions, as illustrated in Figure 2: the UV light triggered the photocuring reaction, aimed at controlling the morphology of the fibers and enhancing the performance of the obtained fibrous membranes.

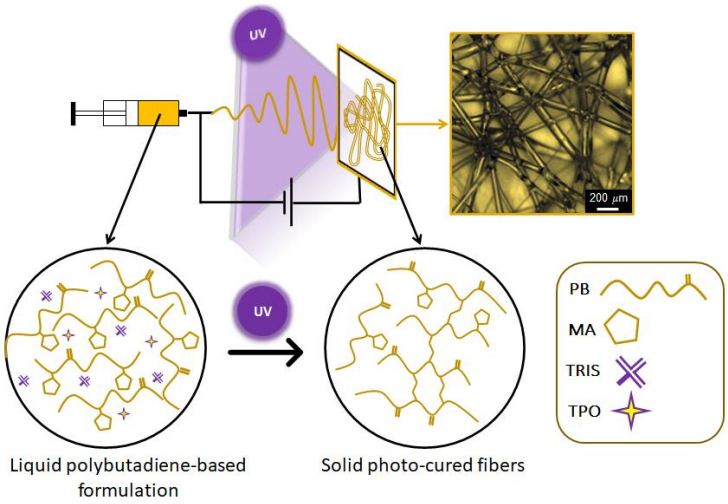

Figure 2. Scheme of the electrospinning process with *in-situ* photocuring of liquid polybutadienes, leading to crosslinked solid fibers.

As liquid oligomers are used, in order to obtain solid fibers on the collector, the photo-crosslinking rate should be compatible with the electrospinning fiber formation speed (a gelification time ≤ 1 s is expected). Thus, the photo-induced curing process was investigated, assessing the solidification rate of the liquid polybutadienes upon UV irradiation in air by measuring their tack-free time (i.e., the irradiation time needed to completely solidify and cure the sample), when in the form of thin films coated onto a glass slide. Tack-free time data of PB, PB-10MA and PB-15MA are reported in Table 2: they varied in the range of few minutes

(3–8 min) for all the investigated samples. Interestingly, liquid polymers having maleic anhydride grafts solidified faster than pure polybutadiene, and the higher was the amount of maleic anhydride, the lower was the solidification time. As a result, the sample containing the highest amount of grafted maleic anhydride (i.e., PB-15MA) showed the fastest photocuring reaction in air.

Table 2. Tack-free time of thin films of liquid polybutadienes due to UV irradiation in air and nitrogen atmosphere: effect of maleic anhydride grafted on the polybutadiene chain.

Sample	Tack-free time (min)	
	Air	Nitrogen
PB	8	12
PB-10MA	5	7
PB-15MA	3	5

For comparison, the same tack-free time tests were carried out by UV irradiation in N_2 atmosphere. The photocuring was faster in air, suggesting the occurrence of crosslinking reactions assisted by oxygen (i.e. the presence of oxidation processes), as will be discussed below. However, the influence of the maleic anhydride group is evident in improving the reactivity under nitrogen as well: in fact, in the presence of such group the light absorption is higher, as assessed by UV-Vis spectroscopy (Figure S1 in the Supplementary Information). Moreover, UV-Vis spectroscopy demonstrated that the maleic anhydride ring is involved in the photocuring reaction also in an inert atmosphere (Figure S1).

The introduction of grafted maleic anhydride moieties on the polybutadiene chain was expected to facilitate the electrospinning by increasing the polymer conductivity and viscosity (Table 1). Accordingly, among the different investigated liquid polybutadiene-based polymers, PB-15MA ($M_n \approx 5750$ g/mol, and ≈15 wt.% of grafted maleic anhydride) was the only one that could form a continuous jet of fibers during electrospinning. In fact, with liquid PB and PB-10MA the electrospinning was not successful (e.g., dripping of the liquid polymer, difficulties in forming the jet, discontinuous jet, flowing of the fibers on the collector) even changing the electrospinning parameters.

However, although PB-15MA underwent the fastest photo-crosslinking (≈ 180 s, see Table 2), the reaction rate was not sufficient to assure a curing time comparable to the polymer jet flying time from the spinneret to the collector. Therefore, the electrospun fibers tended to deform

once they reached the collector, becoming flat and eventually collapsing together (Figure S2 in the Supplementary Information).

To promote the setting of the fiber shape by accelerating the curing reaction, the addition of a radical-type photoinitiator (TPO) and a multifunctional thiol crosslinker (TRIS), which copolymerizes with the polybutadiene carbon-carbon double bonds by a thiol-ene chemistry, was attempted. The effect of the concentration of TPO (1 and 2 wt.%) and TRIS (1.5 and 3 wt.%) on the tack-free time under UV irradiation in air at room temperature was first assessed on PB and PB-15MA thin films: results are reported in Table 3. As expected, for both systems, the solidification time was strongly reduced by the introduction of the photoinitiator (going from 8 to 6 min for PB, and from 3 to around 1 min for PB-15MA, with the addition of 2 wt.% TPO). The introduction of both the photoinitiator and the crosslinker had an even stronger impact on the tack-free time: PB and PB-15MA formulations containing 2 wt.% TPO and 3 wt.% TRIS solidified in few seconds (≤ 5 s) under UV irradiation in air. Thus, while pure liquid polymers were cured in few minutes, the addition of the photoinitiator and the crosslinker led to a faster solidification in a matter of seconds. These curing times were found very promising to perform *in-situ* photocuring of liquid polybutadienes during electrospinning, assuring an adequate solidification of the polymer fibers.

Table 3. Tack-free time of thin films of liquid polybutadienes due to UV irradiation in air: effect of the addition of TPO photoinitiator and TRIS thiol crosslinker.

Sample	Tack-free time (s)
PB–1TPO	480
PB–2TPO	360
PB–2TPO–1.5TRIS	60
PB–2TPO–3TRIS	5
PB-15MA–1TPO	120
PB-15MA–2TPO	65
PB-15MA–2TPO–1.5TRIS	25
PB-15MA–2TPO–3TRIS	< 5

In order to monitor the crosslinking reaction, track the structural changes of the polymer chains during UV irradiation in air, and investigate the effect of the presence of grafted maleic anhydride and of the addition of TPO photoinitiator and TRIS thiol crosslinker on the photocuring, FT-IR spectroscopy was employed. The liquid polymer films were irradiated by UV light, FT-IR spectra were acquired at various time intervals, and the spectra evolution was

monitored (Figure S3–S5 in the Supplementary Information). As an example, Figure 3a and b report the FT-IR spectra of PB and its maleinized homologue PB-15MA at different irradiation times (i.e., 0, 5, 15 min).

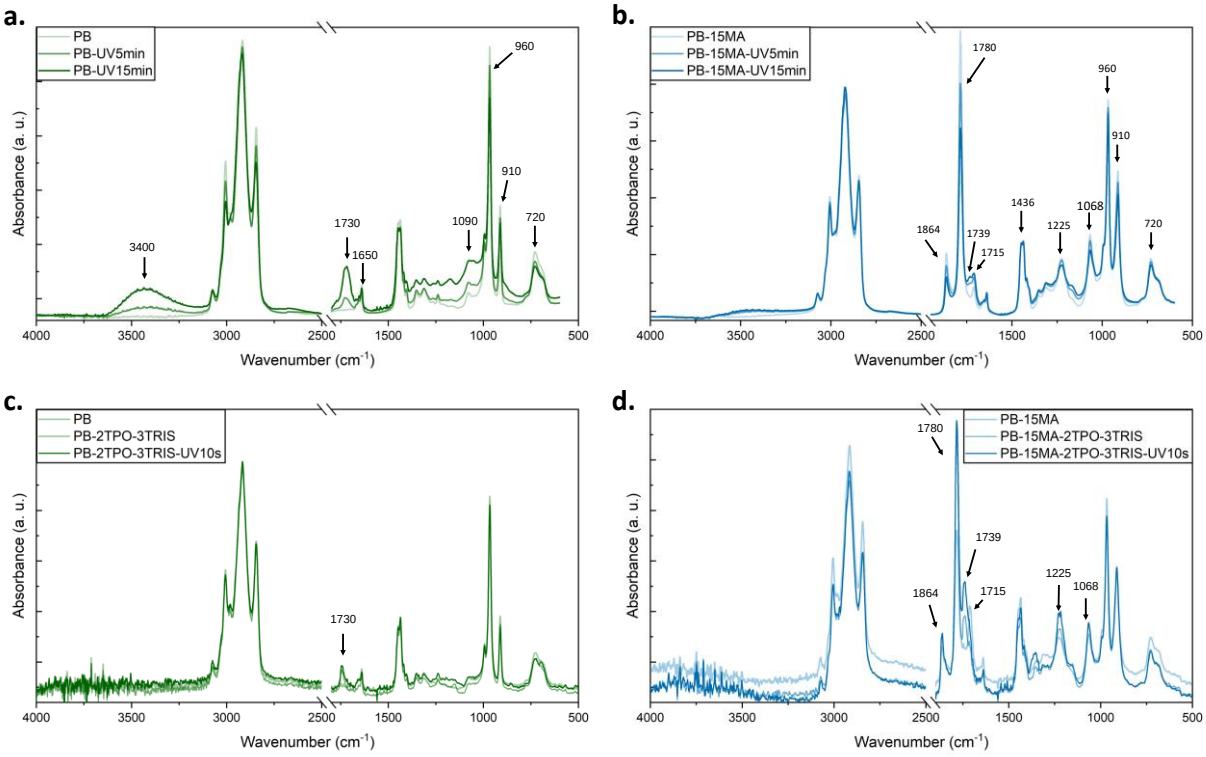

Figure 3. FT-IR spectra of: (a) PB and (b) PB-15MA films prior (irradiation time = 0 min), during (irradiation time = 5 min) and after (irradiation time = 15 min) UV irradiation in air, and (c) PB and (d) PB-15MA films containing 2 wt.% photoinitiator and 3 wt.% crosslinker (PB–2TPO–3TRIS and PB-15MA–2TPO–3TRIS in c and d, respectively) prior (irradiation time = 0 s) and after (irradiation time = 10 s) UV irradiation in air.

As shown in Figure 3a, during irradiation of neat polybutadiene, an important increase of the absorption peaks of the ether (1090 cm^{-1}), carbonyl (1730 cm^{-1}), and hydroxyl (3400 cm^{-1}) groups was detected. This means that PB under UV irradiation in presence of oxygen underwent crosslinking and photo-oxidation reactions, as reported in the literature [47,48,54]. In fact, oxygen molecules can get excited by absorbing UV light, and different reactive oxygen species are generated. These species attack the α-carbons and alkene groups of the PB chains, and hydroperoxide and hydroxyl radicals are thus formed. Such macroradicals can then combine forming a three-dimensional network (photo-crosslinking reaction). Hence, ether linkages between the reactive chains (associated to the peak at 1090 cm^{-1}) increased with UV irradiation time (Figure 3a). A schematic representation of the photo-induced oxygen-mediated crosslinking reaction occurring in the PB system when irradiated in air is proposed in Figure

4a. The photo-crosslinking reaction was also confirmed by the solidification of the liquid PB and its high gel content value (insoluble fraction of 78.6 % after 10 min of irradiation).

The macroradicals on the polymer chains can also combine with oxygen species forming carbonyl and hydroxyl groups. The absorption peak at 1730 cm^{-1}, associated to C=O groups, and the broad band at 3400 cm^{-1}, associated to hydroxyl stretching arising from –OOH or –OH groups [55], grew with irradiation time (Figure 3a), demonstrating not only the appearance of reactive oxygen species responsible for oxygen-mediated crosslinking but also the occurrence of oxidation reactions. Moreover, after UV irradiation, a decrease of the bands at 720 cm^{-1} (out-of-plane deformation of cis –CH=CH–), 960 cm^{-1} (out-of-plane deformation of trans –CH=CH–), 910 cm^{-1} (out-of-plane wagging of $–CH=CH_2$ in the vinyl structure) and 1650 cm^{-1} (stretching of C=C in alkenes) was detected and implied the consumption of double bonds in the PB system.

Comparing the FT-IR spectra of neat PB (Figure 3a) and maleinized PB (Figure 3b) before irradiation, the two peaks at 1780 cm^{-1} and 1864 cm^{-1} in the latter clearly indicated the presence of the carbonyl groups of the maleic anhydride. Moreover, the carbonyl peak at 1715 cm^{-1}, assigned to the C=O bonds of carboxylic acids, revealed the partial opening of the maleic ring. During irradiation of maleinized PB, the peaks at 1780 cm^{-1} and 1864 cm^{-1} decreased, whereas that at 1715 cm^{-1} increased (Figure 3b), indicating further ring opening. Interestingly, upon irradiation, a new band at 1739 cm^{-1}, assigned to the C=O ester groups, also appeared, demonstrating a photo-induced esterification reaction of the anhydride [56–59]. As sketched in Figure 4b, this led to the crosslinking of the polybutadiene chains through the maleic moiety, which occurred together with the crosslinking oxidative reactions of the polybutadiene unsaturations, as discussed before. In fact, the FT-IR spectra of PB-15MA (Figure 3b) showed a decrease of the peaks assigned to the polybutadiene unsaturations (720 cm^{-1}, 910 cm^{-1}, 960 cm^{-1}, and 1650 cm^{-1}) during UV irradiation, indicating the consumption of the double bonds. Whereas the band at 1436 cm^{-1}, assigned to methylene groups $–CH_2–$, increased with irradiation. This is probably due to the gel formation through the crosslinking reaction because of chain reaction and chain transfer mechanisms [48]. In addition, some deformations in the region of the peak bands centered at 1225 cm^{-1} and 1068 cm^{-1}, associated to the symmetric and asymmetric stretching of the ring =C–O–C=, respectively, could be detected.

Therefore, having two concomitant photo-induced curing reactions, i.e., the esterification and the oxidation (Figure 4a and b), the maleinized PB solidified faster than pure PB, as shown by

the tack-free time results (Table 2), leading also to a higher insoluble fraction (i.e., 81.8 % after only 5 min of irradiation).

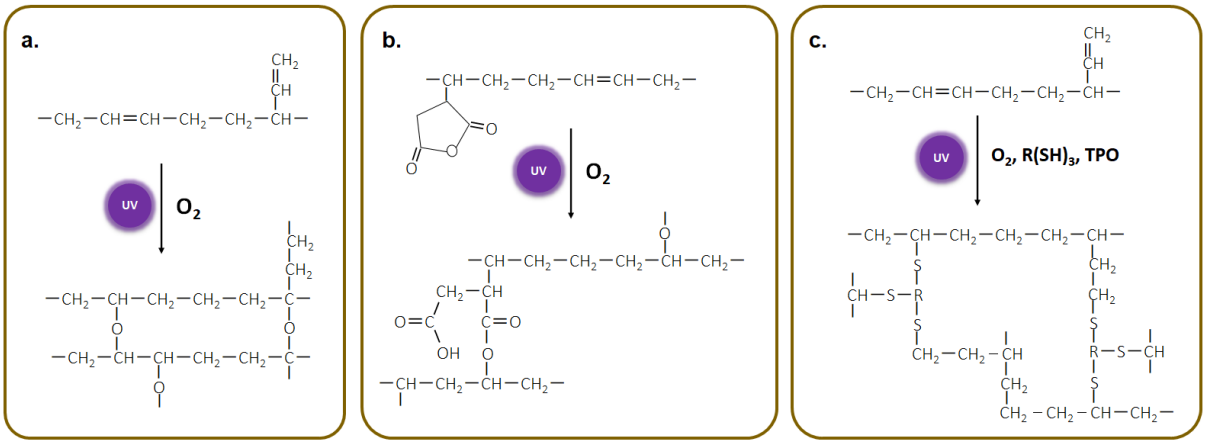

Figure 4. Scheme of the photo-induced crosslinking reactions of PB (a), maleinized PB (b), and polybutadienes in the presence of the trifunctional thiol crosslinker TRIS ($R(SH)_3$) and the photoinitiator TPO (c), occurring during UV irradiation in air.

The crosslinking was further investigated upon addition of the photoinitiator and of the thiol crosslinker. Figure 3c and d report the FT-IR spectra of PB–2TPO–3TRIS and of PB-15MA–2TPO–3TRIS prior and after 10 s of UV irradiation, leading to complete solidification of the films. In this case, the photo-crosslinking reaction was expected to involve the thiol groups of the TRIS crosslinker: however, the consumption of such groups could not be analyzed, as the peak at around 2556 cm^{-1} was not detectable due to its very low intensity (samples contained only 3 wt.% of TRIS). Indeed, a decrease of the peaks assigned to the polybutadiene unsaturations (720 cm^{-1}, 910 cm^{-1}, 960 cm^{-1}, and 1650 cm^{-1}) was observed, as the thiyl radicals react with the backbone butene double bonds as well as with the pendent vinyl double bonds, even when they are in low amount [60].

Interestingly, PB-based sample (Figure 3c) exhibited the appearance of a peak band at 1730 cm^{-1}, assigned to C=O carbonyl bonds (of lower intensity than in the absence of TRIS), but the evolution of the broad peak at 3400 cm^{-1} as a signal for oxidation reactions could not be observed, contrary to what was shown in the absence of the crosslinker (Figure 3a). It can thus be concluded that when a proper photoinitiator and thiol crosslinker are added, the photo-crosslinking of PB, which proceeds readily through intermolecular reactions between functional groups located on different polymer chains, is the main reaction over oxidation.

For PB-15MA–2TPO–3TRIS sample (Figure 3d), upon irradiation, a new band at 1739 cm^{-1} appeared, together with changes to the peaks at 1715 cm^{-1}, 1780 cm^{-1} and 1864 cm^{-1}; as explained above, these modifications indicated the photo-induced esterification reaction of the anhydride. Moreover, some deformations of the peak bands centered at 1225 cm^{-1} and 1068 cm^{-1}, associated to the symmetric and asymmetric stretching of the ring =C–O–C=, respectively, could be detected. Therefore, the photo-induced crosslinking in the presence of oxygen of maleinized polybutadienes added with a thiol crosslinker and a photoinitiator was found to be a multivalent and complex reaction, which concurrently involved the thiol crosslinker links (Figure 4c), the esterification of the maleic anhydride ring and the oxygen-mediated crosslinking of polybutadiene unsaturations, leading to a very fast solidification time.

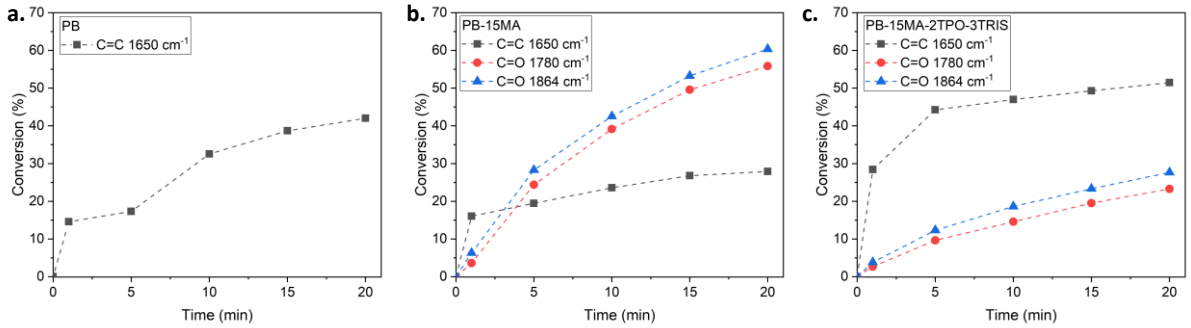

Figure 5. Conversion of C=C functional groups at 1650 cm^{-1} in PB pristine polymer (a) and of C=C functional groups at 1650 cm^{-1} and C=O carbonyl groups of the maleic anhydride at 1780 cm^{-1} and 1864 cm^{-1} in PB-15MA pristine polymer (b) and PB-15MA-2TPO-3TRIS system (c).

Also, the kinetics of crosslinking was analyzed by FT-IR spectroscopy, performed at different irradiation time. In particular, the double bond conversion was monitored through the decrease of the C=C peak at 1650 cm^{-1}, as butene double bonds are only reacting with the thiyl radicals, conversely to vinyl groups that undergo both homopolymerization and copolymerization with the thiol groups [60]. Moreover, the opening of the ring was controlled by tracking the disappearance of the two peaks at 1780 cm^{-1} and 1864 cm^{-1}, assigned to the C=O groups attached to the ring. Conversion results are reported in Figure 5. The conversion of the double bonds on the polymer chain in pristine PB-15MA was found to be lower than for PB system (39% and 27% for PB and PB-15MA, respectively, after 15 min of irradiation). Whereas the disappearance of C=O bonds associated to the maleic anhydride ring was quite high, reaching more than 50 % after 15 min of irradiation. In PB-15MA the crosslinking is thus mainly taking place through the maleic anhydride ring opening. Instead, the addition of the multifunctional

thiol crosslinker and of the photoinitiator leads to a higher contribution of the double bonds on the polybutadiene chains in the crosslinking reaction by the thiol-ene mechanism. In PB-15MA–2TPO–3TRIS system, the C=C conversion was nearly 50% after 15 min of irradiation, while the consumption of C=O did not exceed 25%.

Although the addition of the photoinitiator and the crosslinker greatly accelerated the solidification process for both PB and PB-15MA (Table 3), a small amount of TPO and TRIS significantly decreased the viscosity of the liquid polybutadiene formulations (see below). Therefore, only PB-15MA–2TPO–3TRIS was suitable for electrospinning and *in-situ* UV curing: in this case fibers with a stable morphology were obtained. Thus, this formulation (i.e., PB-15MA–2TPO–3TRIS), exhibiting the fastest solidification time (Table 3) and the best electrospinning performance, was selected for further investigation and characterization.

Firstly, in order to monitor the fast kinetics of the photo-crosslinking of the optimized PB-15MA–2TPO–3TRIS formulation in more detail, as FT-IR spectroscopy did not allow to accurately follow the reaction due to the low intensity of the thiol vibrational band, real-time photo-rheology analyses (i.e., rheology analyses during irradiation) were carried out. Initially, an amplitude sweep experiment was performed to determine the linear viscoelastic region (LVR). Afterwards, a time sweep test at constant strain in the LVR was done, and the UV lamp was switched on after 60 s of data acquisition. As shown in Figure 6, the thiol-ene photo-induced crosslinking reaction was very fast, leading to gelation of PB-15MA–2TPO–3TRIS after 6 s of light irradiation (taken as the time at which G’ and G’’ cross over). In fact, the storage modulus (G’) quickly rose after switching on the UV lamp and after only few seconds predominated the loss modulus (G”). Hence, the UV light irradiation increased the elasticity (G’) of the polymer formulation. This is particularly interesting as a higher degree of elasticity can improve the jet continuity and its elongation [61]. As it can be seen from Figure 6, before irradiation the system exhibited a viscous behavior, while after the UV irradiation it had an elastic behavior with a high G’ plateau.

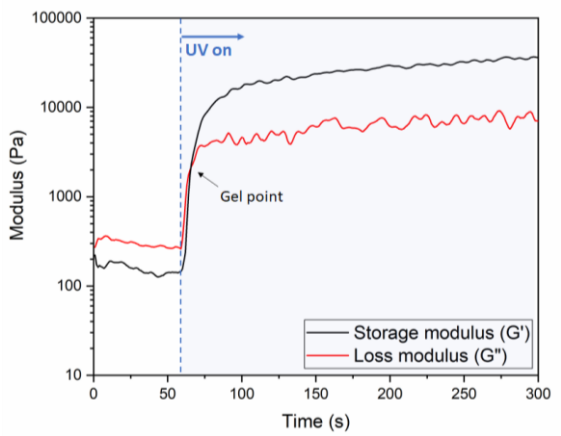

Figure 6. Photo-rheology curve of PB-15MA–2TPO–3TRIS formulation: storage modulus G' and loss modulus G" as a function of time of irradiation; the UV light was switched on after 60 s of measurement.

As comparison, photo-rheology experiments were also performed on the liquid maleinized polybutadiene system containing solely the photoinitiator (PB-15MA–2TPO) or solely the thiol crosslinker (PB-15MA–3TRIS): results are reported in Figure S6 in the Supplementary Information. In these cases, the photo-crosslinking reaction rate was found to be much lower (requiring >90 min and ≈15 min, respectively, to reach the gel point), confirming the importance of the presence of both the photoinitiator and the crosslinker to obtain a very fast curing reaction, meeting the electrospinning process speed.

In order to better control the electrospinning process and reduce the obtained fiber diameters, polar additives can be used. In fact, by reducing the viscoelastic forces, they allow the polymer jet to undergo higher axial stretching during the whipping instability phase [62–64]. Moreover, being easily polarized, they can increase the electrical conductivity governed by mobility of charge carriers or ions, enhancing the charge-carrying capacity of the liquid polymer, favoring the bending instabilities during electrospinning and inducing higher stretching phenomena. Accordingly, polymer mixtures containing a polar additive experience greater repulsive forces, together with stronger stretching forces, leading to more stable electrospinning process [62–64]. In this work, OA was used as polar additive. Prior to electrospinning, the effect of the amount of oleic acid on the formulation viscosity was evaluated by addition of 3, 5 and 9 wt.% OA to the PB-15MA–2TPO–3TRIS sample (Figure 7). It is worth mentioning that the addition of a small amount of crosslinker and photoinitiator reduced the viscosity of the liquid polymer PB-15MA. As shown in Figure 7, the introduction of OA further decreased the viscosity of the system, which passed from 226 Pa s (at a shear rate of 0.01 s^{-1}) to values lower than 100 Pa s (at a shear rate of 0.01 s^{-1}), going from mixtures with no OA to systems with 9 wt.% OA.

However, all the studied formulations showed a viscosity suitable with the electrospinning process [65].

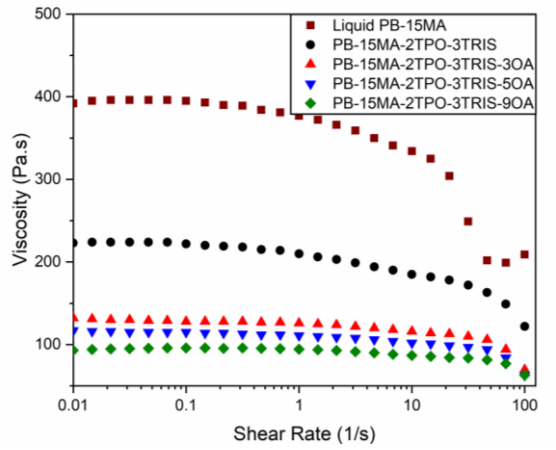

Figure 7. Viscosity vs. shear rate of the pristine PB-15MA, and of PB-15MA–2TPO–3TRIS formulations used in electrospinning with 0, 3, 5 and 9 wt.% OA.

The electrospinning and *in-situ* photo-crosslinking process was successful with all the investigated formulations based on PB-15MA (i.e., PB-15MA–2TPO–3TRIS with 0, 3, 5 and 9 wt.% OA): solid cylindrical fibers were produced in few seconds and collected to form fibrous membranes. It is worth mentioning that the absence of the solvent and accordingly a lower degree of whipping instability and stretching, together with the high viscosity of the PB-15MA formulations at room temperature were expected to yield quite large fibers, as in the range of fibers obtained from melt electrospinning processes [16]. Figure 8 shows the PB-15MA–2TPO–3TRIS electrospun fibrous mat morphology obtained and their fiber diameter distribution. As expected, the addition of OA reduced the fiber diameters: average diameters of 61 µm, 60 µm and 48 µm were obtained for the formulations with 0, 3 and 5 wt.% OA, respectively. However, when the content of OA was 9 wt.%, very large fibers (i.e., average diameter of 115 µm) with a quite wide range of size distribution were produced (Figure 8). In fact, increasing the conductivity of the polymer above a certain level can intensify the instability of the electrospinning process. Anyway, the diameter range of the produced fibers is in well accordance with similar works applying monomer electrospinning and *in-situ* UV curing without solvent [31,32,34].

After preparation, the electrospun mats could be easily detached from the collector, forming free-standing fibrous membranes (Figure S7 in the Supplementary Information).

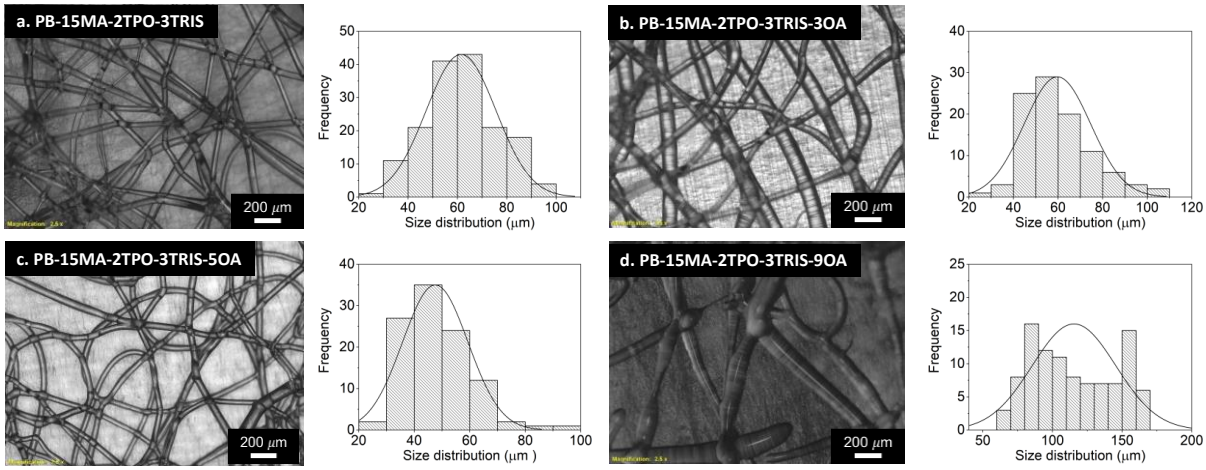

Figure 8. Fiber morphology by optical microscope images of PB-15MA–2TPO–3TRIS formulations with 0 (a), 3 (b), 5 (c) and 9 (d) wt.% OA and their diameter distribution histograms.

The photocuring efficiency as well as the solvent resistance of the different electrospun fiber systems were evaluated by insoluble fraction measurements (Figure S8 in the Supplementary Information). The high gel content values (>80 %) indicated that all fibrous membranes were crosslinked and resistant to solvent. The insoluble fractions slightly decreased with increasing the polar additive content, as it does not take part to the crosslinking reaction and thus remains soluble even after irradiation.

The thermal stability of the different electrospun mats was studied by TGA. As shown in Figure 9a, all samples presented very high thermal resistance. A first small degradation took place at around 250 °C, due to the presence of OA additive, while the major degradation of the photocured membranes occurred after 350 °C (degradation peak centered at around 460 °C). Also analyzing T_5 data (i.e., the temperature at which 5 wt.% of the sample is lost) reported in Table 4, it is clear that the addition of OA lowered the onset temperature of decomposition of the fibers. Whereas T_{50} values (i.e., the temperature at which 50 wt.% of the sample is lost) were found very similar for all investigated systems, in the range 446–449 °C.

Table 4. Degradation temperatures obtained from TGA analyses and Tg obtained by DMTA analyses of crosslinked electrospun PB-15MA–2TPO–3TRIS systems containing 0, 3, 5 and 9 wt.% OA. T_5 and T_{50} are the temperature at which 5 and 50 wt.% of the initial weight is lost, respectively.

Sample	T_5 (°C)	T_{50} (°C)	T_g (°C)
PB-15MA–2TPO–3TRIS	346	449	-58
PB-15MA–2TPO–3TRIS–3OA	265	448	-55
PB-15MA–2TPO–3TRIS–5OA	239	446	-56
PB-15MA–2TPO–3TRIS–9OA	240	446	-

Interestingly, the photo-crosslinked mats were proven to have an exceptional thermal stability of the fibrous morphology. As shown in Figure 9b and 9c, after exposure to elevated temperatures up to 100 °C (see experimental section), the fibers morphology remained unaltered with a slight increase of the fibers diameter (from 60 µm to 77 µm for PB-15MA-2TPO-3TRIS-3OA and from 48 µm to 58 µm for PB-15MA-2TPO-3TRIS-5OA). Moreover, the fiber morphology of the mats was very stable also over time, remaining unchanged for at least one year; only a yellowing process of the membranes could be detected.

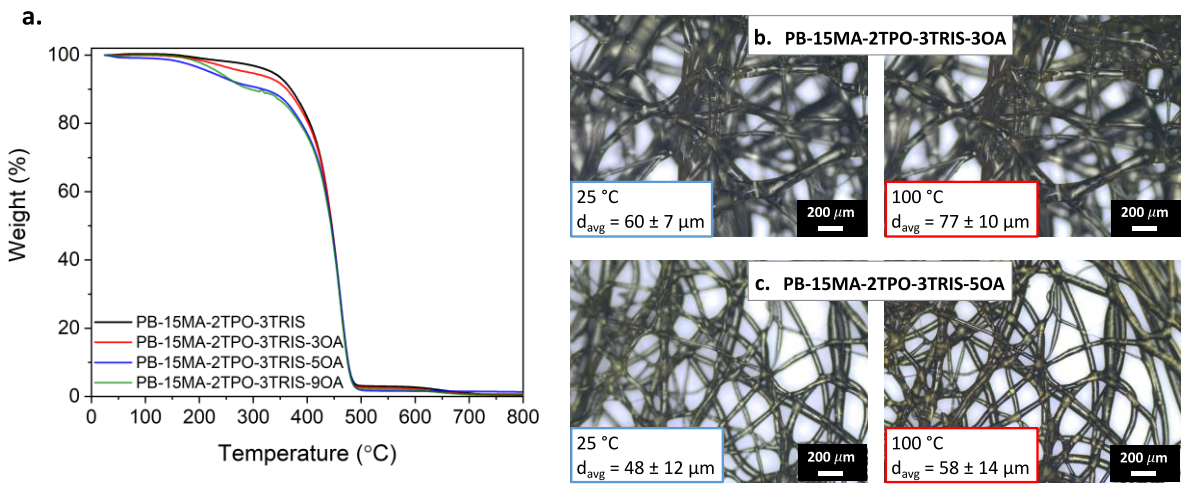

Figure 9. a. TGA thermograms of crosslinked electrospun PB-15MA–2TPO–3TRIS systems containing 0, 3, 5 and 9 wt.% OA. b. and c. Fiber morphology of photocured electrospun PB-15MA–2TPO–3TRIS mats with 3 wt.% OA (b) and 5 wt.% OA (c), before and after a thermal treatment up to 100 °C).

The shape stability of the fibers is particularly remarkable considering that they are characterized by a very low glass transition temperature. The T_g values of the photocured electrospun mats, evaluated by DMTA tests, were comparable for all investigated samples and found approximately at -56 °C (results are reported in Table 4). The electrospun fibers thus maintained their rubber behavior despite the photocuring reaction, which led to a moderate increase of T_g (as the pristine liquid polymer has a T_g=-79°C, measured by DSC, as provided by the supplier). Hence, the crosslinking reaction guaranteed a stable morphology of the fibers but did not modify their rubbery state.

Due to the high surface area of the electrospun mats, their surface properties are of primary importance. The wettability of the photocured fibrous membranes was assessed by static contact angle measurements with water and hexadecane as test liquids. All samples showed very low wettability (contact angle > 80°) when water was used (Figure 10). Whereas contact angle measurements with hexadecane revealed a high oleophilic character of the electrospun

membranes, which showed contact angles close to 0°. These results demonstrating concomitant hydrophobicity and oleophilicity, together with high thermal and morphological stability, are particularly promising for the use of the photocured polybutadiene-based electrospun mats as membranes for water-oil separation.

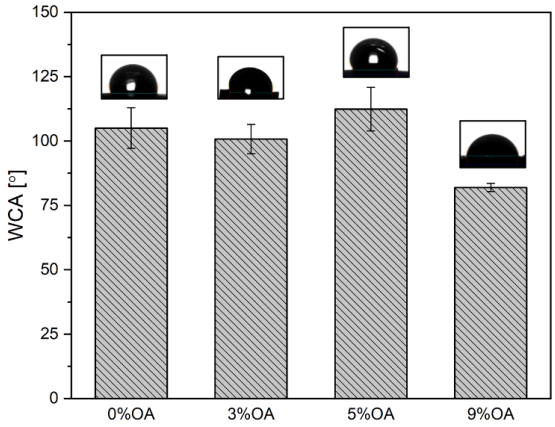

Figure 10. Contact angle with water of the photocured electrospun mats of PB-15MA–2TPO–3TRIS with 0, 3, 5 and 9 wt.% OA.

Conclusions

In view of an increased focus on sustainable production processes of fine fibers, this work describes a technique able to minimize both overall energy consumption from heating (i.e., the entire process is conducted at room temperature) and emission of volatile organic compounds (i.e., no solvents are used). The fabrication of ultrathin rubber fibers was obtained by electrospinning of liquid polybutadienes and their *in-situ* photo-induced crosslinking. As the curing process of the system has to show a fast rate to assure solidification during electrospinning, liquid maleinized PB (polybutadiene-*graft*-maleic anhydride) polymers were used exploiting both the radical abstraction reaction of allylic hydrogen and the photo-induced ring opening of maleic anhydride. However, by employing pure liquid maleinized PB polymers, the fiber morphology of the electrospun mat was not retained. The addition of a photoinitiator (TPO) and of a multifunctional thiol-based crosslinker (TRIS) was thus proposed to achieve suitable photocuring reaction rates. A very fast and complex photo-induced crosslinking reaction, involving at the same time the oxidation of the polybutadiene chains, the esterification of the maleic anhydride moieties and the multifunctional thiol crosslinker, was exploited. Moreover, a polar additive such as oleic acid was introduced in the electrospinning formulations to tune their viscosity and charge density. The liquid polybutadiene-based formulation was optimized, and rubber fibrous membranes with an average fiber diameter of

48 μm were obtained by processing PB-15MA–2TPO–3TRIS with 5 wt.% OA. The membranes showed a remarkably stable morphology over time and temperature changes, high insolubility (insoluble fraction >80 %), good thermal properties (onset temperature of decomposition at ≈250 °C, and major degradation at ≈460 °C), low T_g (-56 °C), and a pronounced hydrophobic and oleophilic character. Moreover, the used method is a single-step approach to easily convert liquid low molecular weight polybutadienes into crosslinked rubber fibers and fibrous membranes in a matter of seconds, without employing solvents and/or heating as requested in spinning a high molecular weight polymer.

Conflicts of interest

There are no conflicts to declare.

Acknowledgements

We acknowledge Synthomer for kindly providing us the liquid polybutadiene polymers.

Supplementary Information

Supplementary information related to this article is available.

Data availability

The raw/processed data required to reproduce these findings cannot be shared at this time as the data also forms part of an ongoing study.

References

[1] D.H. Reneker, I. Chun, Nanometre diameter fibres of polymer, produced by electrospinning, Nanotechnology. 7 (1996) 216.

[2] Z.M. Huang, Y.Z. Zhang, M. Kotaki, S. Ramakrishna, A review on polymer nanofibers by electrospinning and their applications in nanocomposites, Compos. Sci. Technol. 63 (2003) 2223–2253. https://doi.org/10.1016/S0266-3538(03)00178-7.

[3] N. Bhardwaj, S.C. Kundu, Electrospinning: A fascinating fiber fabrication technique, Biotechnol. Adv. 28 (2010) 325–347.

https://doi.org/10.1016/j.biotechadv.2010.01.004.

[4] W.E. Teo, S. Ramakrishna, A review on electrospinning design and nanofibre assemblies, Nanotechnology. 17 (2006) R89.

[5] Q. Liu, J. Zhu, L. Zhang, Y. Qiu, Recent advances in energy materials by electrospinning, Renew. Sustain. Energy Rev. 81 (2018) 1825–1858.

[6] R. Dersch, M. Steinhart, U. Boudriot, A. Greiner, J.H. Wendorff, Nanoprocessing of polymers: applications in medicine, sensors, catalysis, photonics, Polym. Adv. Technol. 16 (2005) 276–282.

[7] K. Chen, W. Chou, L. Liu, Y. Cui, P. Xue, M. Jia, Electrochemical sensors fabricated by electrospinning technology: an overview, Sensors. 19 (2019) 3676.

[8] Y. Sun, S. Cheng, W. Lu, Y. Wang, P. Zhang, Q. Yao, Electrospun fibers and their application in drug controlled release, biological dressings, tissue repair, and enzyme immobilization, RSC Adv. 9 (2019) 25712–25729.

[9] H. Liu, C.R. Gough, Q. Deng, Z. Gu, F. Wang, X. Hu, Recent Advances in Electrospun Sustainable Composites for Biomedical, Environmental, Energy, and Packaging Applications, Int. J. Mol. Sci. 21 (2020) 4019.

[10] E. Mele, Electrospinning of natural polymers for advanced wound care: towards responsive and adaptive dressings, J. Mater. Chem. B. 4 (2016) 4801–4812.

[11] R. Chen, Y. Wan, W. Wu, C. Yang, J.-H. He, J. Cheng, R. Jetter, F.K. Ko, Y. Chen, A lotus effect-inspired flexible and breathable membrane with hierarchical electrospinning micro/nanofibers and ZnO nanowires, Mater. Des. 162 (2019) 246–248. https://doi.org/https://doi.org/10.1016/j.matdes.2018.11.041.

[12] J. Xue, T. Wu, Y. Dai, Y. Xia, Electrospinning and electrospun nanofibers: Methods, materials, and applications, Chem. Rev. 119 (2019) 5298–5415. https://doi.org/10.1021/acs.chemrev.8b00593.

[13] D.H. Reneker, A.L. Yarin, H. Fong, S. Koombhongse, Bending instability of electrically charged liquid jets of polymer solutions in electrospinning, J. Appl. Phys. 87 (2000) 4531–4547.

[14] R. Deng, Y. Liu, Y. Ding, P. Xie, L. Luo, W. Yang, Melt electrospinning of low-density polyethylene having a low-melt flow index, J. Appl. Polym. Sci. 114 (2009) 166–175.

[15] A. Gora, R. Sahay, V. Thavasi, S. Ramakrishna, Melt-electrospun fibers for advances in biomedical engineering, clean energy, filtration, and separation, Polym. Rev. 51 (2011) 265–287.

[16] J. Lyons, C. Li, F. Ko, Melt-electrospinning part I: processing parameters and geometric properties, Polymer (Guildf). 45 (2004) 7597–7603.

[17] N. Ogata, N. Shimada, S. Yamaguchi, K. Nakane, T. Ogihara, Melt-electrospinning of poly (ethylene terephthalate) and polyalirate, J. Appl. Polym. Sci. 105 (2007) 1127–1132.

[18] P.D. Dalton, J. Lleixà Calvet, A. Mourran, D. Klee, M. Möller, Melt electrospinning of poly-(ethylene glycol-block-ϵ-caprolactone), Biotechnol. J. Healthc. Nutr. Technol. 1 (2006) 998–1006.

[19] D. Lv, M. Zhu, Z. Jiang, S. Jiang, Q. Zhang, R. Xiong, C. Huang, Green electrospun nanofibers and their application in air filtration, Macromol. Mater. Eng. 303 (2018) 1800336.

[20] N. Corrigan, J. Yeow, P. Judzewitsch, J. Xu, C. Boyer, Seeing the light: advancing materials chemistry through photopolymerization, Angew. Chemie Int. Ed. 58 (2019) 5170–5189.

[21] G. Fredi, P. Kianfar, S. Dalle Vacche, A. Pegoretti, A. Vitale, Electrospun Shape-Stabilized Phase Change Materials Based on Photo-Crosslinked Polyethylene Oxide, Polym. . 13 (2021). https://doi.org/10.3390/polym13172979.

[22] P. Kianfar, A. Vitale, S. Dalle Vacche, R. Bongiovanni, Enhancing properties and water resistance of PEO-based electrospun nanofibrous membranes by photo-crosslinking, J. Mater. Sci. 56 (2020) 1879–1896.

[23] P. Kianfar, A. Vitale, S. Dalle Vacche, R. Bongiovanni, Photo-crosslinking of chitosan/poly(ethylene oxide) electrospun nanofibers, Carbohydr. Polym. 217 (2019) 144–151. https://doi.org/10.1016/j.carbpol.2019.04.062.

[24] P. Ferreira, P. Santos, P. Alves, M.P. Carvalho, K.D. de Sá, S.P. Miguel, I.J. Correia, P. Coimbra, Photocrosslinkable electrospun fiber meshes for tissue engineering applications, Eur. Polym. J. 97 (2017) 210–219.

[25] L. Jun, Y. Zhang, Y. Hao, L. Cheng, Z. JJ, Preparation of porous electro-spun UPM fibers via photocrosslinking, J. Appl. Polym. Sci. 112 (2009) 2247–2254.

[26] A.R. Tan, J.L. Ifkovits, B.M. Baker, D.M. Brey, R.L. Mauck, J.A. Burdick, Electrospinning of photocrosslinked and degradable fibrous scaffolds, J. Biomed. Mater. Res. Part A An Off. J. Soc. Biomater. Japanese Soc. Biomater. Aust. Soc. Biomater. Korean Soc. Biomater. 87 (2008) 1034–1043.

[27] S.S. Choi, J.P. Hong, Y.S. Seo, S.M. Chung, C. Nah, Fabrication and characterization of electrospun polybutadiene fibers crosslinked by UV irradiation, J. Appl. Polym. Sci. 101 (2006) 2333–2337. https://doi.org/10.1002/app.23764.

[28] M.W. Thielke, E.P. Bruckner, D.L. Wong, P. Theato, Thiol-ene modification of electrospun polybutadiene fibers crosslinked by UV irradiation, Polymer (Guildf). 55 (2014) 5596–5599.

[29] K. Shanmuganathan, R.K. Sankhagowit, P. Iyer, C.J. Ellison, Thiol–ene chemistry: a greener approach to making chemically and thermally stable fibers, Chem. Mater. 23 (2011) 4726–4732.

[30] K. Shanmuganathan, S.M. Elliot, A.P. Lane, C.J. Ellison, Highly Stretchable Thermoset Fibers and Nonwovens Using Thiol–ene Photopolymerization, ACS Appl. Mater. Interfaces. 6 (2014) 14259–14265.

[31] H.-W. He, L. Wang, X. Yan, L.-H. Zhang, M. Yu, G.-F. Yu, R.-H. Dong, L.-H. Xia, S. Ramakrishna, Y.-Z. Long, Solvent-free electrospinning of UV curable polymer microfibers, RSC Adv. 6 (2016) 29423–29427.

[32] L. Wang, H.-W. He, X. Yan, G.-F. Yu, X.-S. Jia, J.-T. Li, L.-H. Xia, X. Ning, Y.-Z. Long, Ecofriendly fabrication of ultrathin colorful fibers via UV-assisted solventless electrospinning, RSC Adv. 6 (2016) 86597–86601.

[33] Y. Fang, A.R. Dulaney, J. Gadley, J. Maia, C.J. Ellison, A comparative parameter study: Controlling fiber diameter and diameter distribution in centrifugal spinning of

photocurable monomers, Polymer (Guildf). 88 (2016) 102–111.

[34] X.-X. He, G.-F. Yu, X.-X. Wang, J. Zhang, J. Zheng, M. Yu, X. Ning, Y.-Z. Long, Electromagnetic functionalized micro-ribbons and ropes for strain sensors via UV-assisted solvent-free electrospinning, J. Phys. D. Appl. Phys. 50 (2017) 395601.

[35] X. Zhu, Q. Niu, Y. Xu, G. Wu, G. Li, J. Nie, G. Ma, From small molecules to polymer fibers: Photopolymerization with electrospinning on the fly, J. Photochem. Photobiol. A Chem. 353 (2018) 101–107.

[36] S.-S. Kim, C.M. Lau, L.M. Lillie, W.B. Tolman, T.M. Reineke, C.J. Ellison, Degradable Thermoset Fibers from Carbohydrate-Derived Diols via Thiol–Ene Photopolymerization, ACS Appl. Polym. Mater. 1 (2019) 2933–2942.

[37] H. Fong, D.H. Reneker, Elastomeric nanofibers of styrene–butadiene–styrene triblock copolymer, J. Polym. Sci. Part B Polym. Phys. 37 (1999) 3488–3493.

[38] T.E. Kerr-Phillips, V. Woehling, R. Agniel, G.T.M. Nguyen, F. Vidal, P. Kilmartin, C. Plesse, J. Travas-Sejdic, Electrospun rubber fibre mats with electrochemically controllable pore sizes, J. Mater. Chem. B. 3 (2015) 4249–4258.

[39] X. Zhang, G.G. Chase, Electrospun elastic acrylonitrile butadiene copolymer fibers, Polymer (Guildf). 97 (2016) 440–448.

[40] H.C. Duong, D. Chuai, Y.C. Woo, H.K. Shon, L.D. Nghiem, V. Sencadas, A novel electrospun, hydrophobic, and elastomeric styrene-butadiene-styrene membrane for membrane distillation applications, J. Memb. Sci. 549 (2018) 420–427.

[41] J. Yoon, J. Lee, J. Hur, Stretchable supercapacitors based on carbon nanotubes-deposited rubber polymer nanofibers electrodes with high tolerance against strain, Nanomaterials. 8 (2018) 541.

[42] A. Vitale, G. Massaglia, A. Chiodoni, R. Bongiovanni, C.F. Pirri, M. Quaglio, Tuning Porosity and Functionality of Electrospun Rubber Nanofiber Mats by Photo-Crosslinking, ACS Appl. Mater. Interfaces. 11 (2019) 24544–24551.

[43] G.-Y. Li, J.L. Koenig, A review of rubber oxidation, Rubber Chem. Technol. 78 (2005) 355–390.

[44] L.-W. Chen, T. Nemoto, J. Kumanotani, Oxidative Polymerization of Polybutadiene and Its Derivatives, Bull. Chem. Soc. Jpn. 40 (1967) 747–751.

[45] M. Mehrabzadeh, S. Kasaei, M. Khosravi, Modification of fast-cure ethylene–propylene diene terpolymer rubber by maleic anhydride and effect of electron donor, J. Appl. Polym. Sci. 70 (1998) 1–5.

[46] P.A. Nelson, S.K.N. Kutty, Cure characteristics and mechanical properties of maleic anhydride grafted reclaimed rubber/styrene butadiene rubber blends, Polym. Plast. Technol. Eng. 43 (2004) 245–260.

[47] P.O. Bussière, J.L. Gardette, J. Lacoste, M. Baba, Characterization of photodegradation of polybutadiene and polyisoprene: Chronology of crosslinking and chain-scission, Polym. Degrad. Stab. 88 (2005) 182–188. https://doi.org/10.1016/j.polymdegradstab.2004.02.013.

[48] V.T. Kagiya, K. Takemoto, Crosslinking and oxidation of 1, 2-Polybutadiene by UV irradiation, J. Macromol. Sci. 10 (1976) 795–810.

[49] N. Ten Brummelhuis, C. Diehl, H. Schlaad, Thiol-Ene modification of 1,2-polybutadiene using UV light or sunlight, Macromolecules. 41 (2008) 9946–9947. https://doi.org/10.1021/ma802047w.

[50] M. Desroches, S. Caillol, V. Lapinte, R. Auvergne, B. Boutevin, Synthesis of biobased polyols by thiol− ene coupling from vegetable oils, Macromolecules. 44 (2011) 2489–2500.

[51] C. Decker, T.N.T. Viet, Photocrosslinking of functionalized rubbers, 7. Styrene-butadiene block copolymers, Macromol. Chem. Phys. 200 (1999) 358–367.

[52] C.E. Hoyle, C.N. Bowman, Thiol–ene click chemistry, Angew. Chemie Int. Ed. 49 (2010) 1540–1573.

[53] ASTM D1640/D1640M-14, ASTM D1640/D1640M-14, Standard Test Methods for Drying, Curing, or Film Formation of Organic Coatings, 2018. https://doi.org/10.1520/D1640_D1640M-14R18.

[54] I. Schopov, N. Kassabova, G. Kossmehl, Oxidation of cis-1, 4-polybutadiene by singlet oxygen, Polym. Degrad. Stab. 25 (1989) 31–38.

[55] J. Lee, B. Moon, Synthesis of telechelic anthraquinone-functionalized polybutadiene via ROMP and study of its photo-oxidation and UV crosslinking behaviors, J. Polym. Sci. Part A Polym. Chem. 56 (2018) 1249–1258.

[56] J. Sheng, X.L. Lu, K. De Yao, Investigation of graft polymerization of maleic anhydride onto polybutadiene rubber, J. Macromol. Sci. Part A - Chem. 27 (1990) 167–178. https://doi.org/10.1080/00222339009351494.

[57] S. Yamamoto, R.A. Back, The thermal and photochemical decompositions of succinic anhydride and 2, 3-dimethyl succinic anhydride in the gas phase, Can. J. Chem. 61 (1983) 2790–2794.

[58] P.E. Watkins, E. Whittle, Photochemistry of anhydrides. Part 5.—Photolysis of perfluorosuccinnic anhydride, J. Chem. Soc. Faraday Trans. 1 Phys. Chem. Condens. Phases. 76 (1980) 503–511.

[59] B. Dinda, Photochemistry of Aromatic Compounds, in: Essentials Pericyclic Photochem. React., Springer, 2017: pp. 277–299.

[60] C. Decker, T.N.T. Viet, Photocrosslinking of functionalized rubbers, 8. The thiol-polybutadiene system, Macromol. Chem. Phys. 200 (1999) 1965–1974.

[61] H.Y. Jian, S. V Fridrikh, G.C. Rutledge, The role of elasticity in the formation of electrospun fibers, Polymer (Guildf). 47 (2006) 4789–4797.

[62] R.M. Nezarati, M.B. Eifert, E. Cosgriff-Hernandez, Effects of humidity and solution viscosity on electrospun fiber morphology, Tissue Eng. - Part C Methods. 19 (2013) 810–819. https://doi.org/10.1089/ten.tec.2012.0671.

[63] R. Nayak, R. Padhye, I.L. Kyratzis, Y.B. Truong, L. Arnold, Effect of viscosity and electrical conductivity on the morphology and fiber diameter in melt electrospinning of polypropylene, Text. Res. J. 83 (2013) 606–617. https://doi.org/10.1177/0040517512458347.

[64] C. Zhiyuan, J. He, Z. Fengwen, L. Yuexing, L. Yong, Y. Huilin, Effect of polar additives on melt electrospinning of nonpolar polypropylene, J. Serbian Chem. Soc. 79 (2014) 587–596.

[65] A. Bachs-Herrera, O. Yousefzade, L.J. del Valle, J. Puiggali, Melt electrospinning of

polymers: Blends, nanocomposites, additives and applications, Appl. Sci. 11 (2021) 1808.